Ultra low-noise differential ac-coupled photodetector for sensitive pulse detection applications



2009 Meas. Sci. Technol. 20 055301

(http://iopscience.iop.org/0957-0233/20/5/055301)

Meas. Sci. Technol. **20** (2009) 055301 (7pp) doi:10.1088/0957-0233/20/5/055301

# Ultra low-noise differential ac-coupled photodetector for sensitive pulse detection applications

**Patrick J Windpassinger[1,3], Marcin Kubasik[2,4], Marco Koschorreck[2], Axel Boisen[1], Niels Kjærgaard[1], Eugene S Polzik[1] and Jörg Helge Müller[1]**

[1] QUANTOP, Niels Bohr Institute, University of Copenhagen, Blegdamsvej 17, 2100 Copenhagen, Denmark
[2] ICFO-Institut de Ciencies Fotoniques, Mediterranean Technology Park, 08860 Castelldefels (Barcelona), Spain

E-mail: pwindpas@nbi.dk

Received 3 November 2008, in final form 19 February 2009
Published 17 April 2009
Online at stacks.iop.org/MST/20/055301

**Abstract**
We report on the performance of ultra low-noise differential photodetectors especially designed for probing of atomic ensembles with weak light pulses. The working principle of the detectors is described together with the analysis procedures employed to extract the photon shot noise of light pulses with $\sim$1 $\mu$s duration. As opposed to frequency response peaked detectors, our approach allows for broadband quantum noise measurements. The equivalent noise charge (ENC) for two different hardware approaches is evaluated to 280 and 340 electrons per pulse, respectively, which corresponds to a dark noise equivalent photon number of $n_{3\mathrm{dB}} = 0.8 \times 10^5$ and $n_{3\mathrm{dB}} = 1.2 \times 10^5$ in the two approaches. Finally, we discuss the possibility of removing classical correlations in the output signal caused by detector imperfection by using double-correlated sampling methods.

**Keywords:** optical detectors, electrical noise, quantum noise

(Some figures in this article are in colour only in the electronic version)

## 1. Introduction

Many experiments in the area of atomic physics and quantum information science hinge on the possibility of detecting light pulses of a few microseconds duration with low photon numbers ($n_{\mathrm{ph}} \sim 10^5$) reliably, i.e., with ideally no noise contribution from the detection electronics. For example, in the specific case of interferometric measurements [1–4], small differential signals in the interferometer outputs need to be measured with quantum noise limited precision. Strong local oscillators are in principle possible in some of these set-ups, however, especially when interested in measuring broadband quantum noise, low-noise detectors greatly relax the requirements on the technical noise of the local oscillator. The need for very low-noise analog photodetectors becomes even more apparent, when the number of photons needs to be measured in a pulse with a photon flux too high to employ direct photon counting techniques [5]. In general, any application where the number of photons to probe a system is limited, e.g. to minimize the energy deposited into a system in spectroscopy, will benefit from low detection noise.

In the following, we discuss the performance of photodetectors employed to faithfully measure the photon number difference of two light beams. The difference in photon numbers of light pulses with known shape and arrival time at the detector will contain the information we wish to retrieve. The information should preferably be extracted with a precision only limited by the intrinsic quantum fluctuations of light—light shot noise. Hence electronic and classical noise contributions should be suppressed as much as possible. To

[3] Present address: Institut für Laserphysik, Luruper Chaussee 149, 22761 Hamburg, Germany.
[4] Present address: Clarendon Laboratory, Parks Road, Oxford OX1 3PU, UK.

 

**Table 1.** Comparison of the two detector versions.

| | Version I AMPTEK | Version II Cremat |
|---|---|---|
| Integrator | A250, external FET and feedback | CR 110, hybrid |
| Shaper | 2 × A275, 3 pole, 330 ns | CR-200-250 ns, hybrid |
| $n_{\text{photon,3dB}}$ | $0.8 \times 10^5$ | $1.2 \times 10^5$ |

this end, we have developed differential photodetectors based on two different commercially available front-end hybrid amplifiers. In Version I we use a similar layout as discussed in [6], based on Amptek[3] amplifiers. Version II is based on a charge sensitive preamplifier and a pulse shaping module from Cremat[4]. The differences and performances are compared in table 1.

These detectors were designed for the purpose of measuring quantum noise in atomic ensembles [7]; therefore both the photon number impinging on the detector and the duration of the light pulses are restricted by the optical depth and the coherence time of the ensemble [4] to the range of $10^5$–$10^6$ photons per microsecond. We have built several units of each type and with both approaches we consistently reach electronic noise levels of ENC $\sim$ 300 for input pulse durations $\tau \lesssim 1\ \mu$s. We thus demonstrate an extension of the technique proposed in [6] to the microsecond domain (compared to picoseconds). Despite the longer pulses in our measurements, we achieve an improvement of the noise performance by a factor of 2–2.5 with respect to [6]. We start out by briefly reviewing the working principle of the detectors. The data analysis procedures are discussed in detail and the detector performance is evaluated.

## 2. Technical background

A schematic block diagram of the detector circuits we consider is shown in figure 1. The current through two biased PIN photodiodes (Hamamatsu S3883) is directly subtracted and the difference current is ac coupled into a charge sensitive amplifier. The node between the photodiodes is in some implementations connected with high resistance (50 MΩ–1 GΩ) to the midpoint of the supply voltages in order to avoid large difference in bias voltage for diodes with differing dark currents. In Version I, the charge integrator is built with a discrete external FET input stage coupled to a high-speed operational amplifier (AMPTEK A250) using external R-C-feedback. In Version II a self-contained unit (Cremat CR110) with similar functionality but fixed integration gain is used. The integrated signal is buffered and derived with Gaussian filters (shaping amplifiers), where the shaping time of Version I is user defined. Version II features an integrated shaper circuit module with fixed shaping time (Cremat CR200) of 250 ns. Typical signals at different stages in the detector for 1 $\mu$s unbalanced input light pulses are shown as insets in figure 1. The high gain–bandwidth product and fast slew rate of the amplifiers in the integrator circuit set the minimum rise time at the integrator output to $\sim$5 ns. A pulse with a duration of more than the rise time will be transformed into a linearly rising voltage at the output of the integrator, where the slope is proportional to the differential photo current and the total step size proportional to the total (differential) charge. The discharging time $\tau_i = C_i R_i$ of the integrator feedback circuit is chosen such that it has little influence during the actual light pulse, $\tau_i \gg \tau$.

Deriving the integrated signal with a Gaussian filter, in the simplest form realized by a C-R–R-C combination as indicated in figure 1, will result in a pulse with an area proportional to the integrated charge. For input pulses considerably shorter than the shaping time of the filters, the duration of the output pulse will be approximately 2.4 the shaping time with now both pulse height and pulse area proportional to the integrated charge. This is the usual mode of operation for charge sensitive front-ends in x-ray and particle detectors. An initial light pulse with a duration longer than the shaping time will result in an output signal which is widened approximately by twice the shaping time. In our particular implementation the shaping time of Version I is set to 330 ns, thus a light pulse of $\tau \approx 100$ ns duration will result in an electronic pulse of $\sigma \approx 800$ ns. Figure 2 shows output pulse samples for unbalanced rectangular input light pulses of various durations incident on the detector. It should be clear that the type of integrating detector presented here is not suited to provide information about the temporal shape of the input signal on a time scale shorter than the shaping time. The choice of a specific shaping time is a compromise between the desired time resolution and the digital signal sampling bandwidth for postprocessing of the data. The input referred electronic noise level in the chosen amplifier configuration depends essentially on the combined size of detector capacitance and the gate capacitance of the input FET [8]. In addition, there is a dependence of the noise on shaping time and the digital postprocessing. In the remainder of this paper, we will characterize the output referred noise level in different operating regimes.

In the simple Gaussian filter configuration, an active C-R–R-C high–low pass combination, the output level of the electronic signal restores to zero only on the timescale of the integrator discharge time $\tau_i$. More formally, the transfer function of the combined system has a pole at $\tau_i$ which leads to a nonzero signal after the pulse. The pole in the transfer function of the integrator can be compensated for by adding a zero in the transfer function of the subsequent filter. This is achieved by adding the resistor $R_{\text{P/Z}}$ shown in figure 1. Adapting the resistor value to the preceding integrator allows us to reduce the effect of the pole. In practice, the cancellation is never perfect leading to weak but long tails (baseline pulling or pulse pile-up) in the detector response. This imperfection is evident in figure 2 for pulses with durations longer than 1 $\mu$s. It has to be accounted for properly in the analysis since it is proportional to the input pulse photon number and thus can enter as a classical noise contribution (autocorrelation) in a statistical analysis of pulse areas from trains of pulses. Under ideal conditions, the average detector signal is balanced to zero at all times and the noise is calculated from fluctuations

[5] Amptek Inc., 14 De Angelo Drive, Bedford, MA 01730, USA.
[6] Cremat Inc., 45 Union St, Watertown, MA 02472, USA.

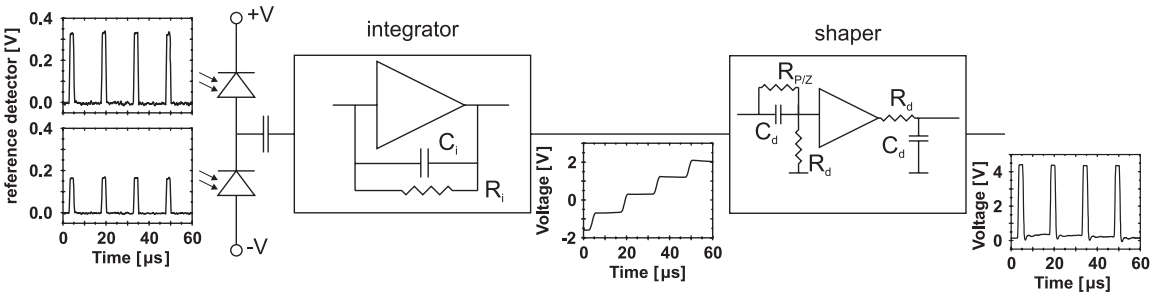


**Figure 1.** Schematics of the detector electronics. When an imbalanced signal is applied to the directly subtracted photodiodes as shown on the left, the differential photoelectrons are integrated. The time constant of the differentiator is adjusted such that it matches the decay time of the integrator. In consequence, the signal is zero between the pulses and the integral of the output pulses after the shaper is proportional to the differential photoelectrons.

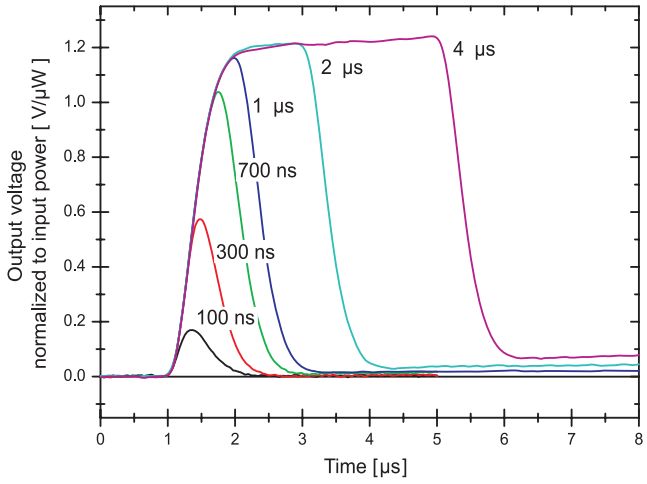


**Figure 2.** Output signal samples for different input pulse durations. The output signal has been normalized to the power of the input beam. The duration of the electronic output signal is extended by twice the shaping time. For long pulses, i.e. high photon numbers per pulse, a clear pulling of the detector baseline can be observed as an output signal which does not coincide with the level prior to the pulse.

around the zero level. In practice, drifts in the optical set-up can lead to slowly varying signal imbalance over time and cause considerable contributions for baseline pileup.

To analyze the output signal of the detectors, we use a digital storage oscilloscope (Agilent Infiniium 54832D) with analog bandwidth limitation to 20 MHz to avoid undersampling and folding of RF interference. The signal trace is digitized and stored for numerical postprocessing. By treating the electronic signal in this way, the only additional noise contribution after the detector front-end originates from the input channel noise of the oscilloscope and the digitization noise of the 8 bit A/D converter. With high gain in the front-end and by choosing equipment of suitable quality, these noise sources can be neglected.

## 3. Noise analysis and detector performance

### *3.1. CW noise spectra and time-domain integration*

We model the light pulses incident on the detector as coherent state excitations with a temporal mode function given by the

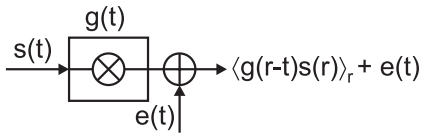


**Figure 3.** Block diagram of the circuit. The gain function $g(t)$ acts on the incoming signal $s(t)$ and the output referenced noise is included as a random signal $e(t)$.

rectangular pulse envelope. Denoting the coherent light state as $|\alpha\rangle$, one has a mean photon number $\langle\alpha|\hat{N}|\alpha\rangle = \langle\alpha|a^\dagger a|\alpha\rangle = \bar{N}$ in every pulse and intrinsic Poissonian fluctuations of size$\langle(\delta\hat{N})^2\rangle = \langle\alpha|(\hat{N}-\bar{N})^2|\alpha\rangle = \bar{N}$ from pulse to pulse [9]. Thus, the expected noise (variance) of a measurement is equal to the mean number of photons in the pulse. This picture remains valid when a single coherent state with $\bar{N}$ photons is split into two $\bar{N}_1+\bar{N}_2 = \bar{N}$ on a beam splitter and both coherent states are measured individually. The variance of the combined output signal—e.g. balanced difference detection of the two states as in our case—will still be $\langle(\delta(\hat{N}_1-\hat{N}_2))^2\rangle = \bar{N}$. As a typical feature of quantum noise, the variance of the output signal of the balanced detector should thus scale linearly with the mean photon number per pulse.

To describe the noise properties of the detector, we consider the block diagram shown in figure 3. The input signal is characterized by the random variable $s(t)$. The detector gain $g(t)$ only acts on the input signal and the output corresponds to the convolution of the two processes, $o(t) = \langle g(r-t)s(r)\rangle_r$. We add a random electronic signal $e(t)$ at the output to account for the dark detector noise. The term noise is usually connected to the autocorrelation function $\Omega(t) = \langle o(r)o(r-t)\rangle_r$ of a time-dependent random signal $o(t)$ or the Fourier transform of the autocorrelation function $\Omega(\omega)$, which is the so-called spectral noise power density. According to the Wiener–Khinchin theorem, $\Omega(\omega) = \langle|o(\omega)|^2\rangle$, where $o(\omega)$ is the Fourier transform of $o(t)$ [10]. Consequently, when invoking Parseval's theorem, the spectral noise power density which can conveniently be measured on a spectrum analyzer can be converted into

$$\Omega(\omega) = |g(\omega)|^2|s(\omega)|^2 + |e(\omega)|^2. \quad (1)$$

Modeling a primary detection event as a $\delta$-function current spike at the input implies a flat spectral noise power density $|s(\omega)|^2 = s_0$ (white noise) with a strength directly proportional

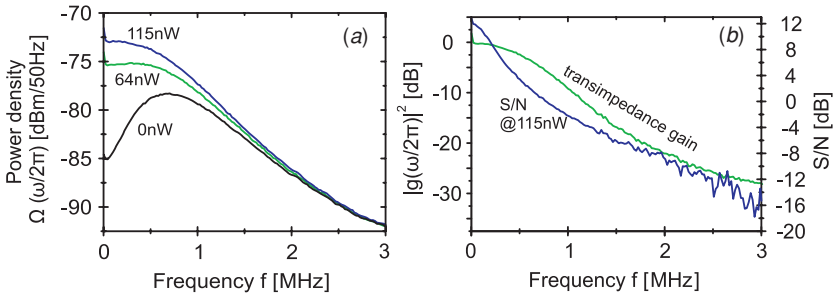


**Figure 4.** (*a*) Power spectrum of the detector when different, balanced dc light power levels are applied to the detector. (*b*) Frequency response of the detector, calculated from the raw data trace in (*a*) at 115 nW dc light power level. The gain drops by 3 dB within ∼600 kHz, which corresponds well to a shaping time of ∼1.5 $\mu$s.

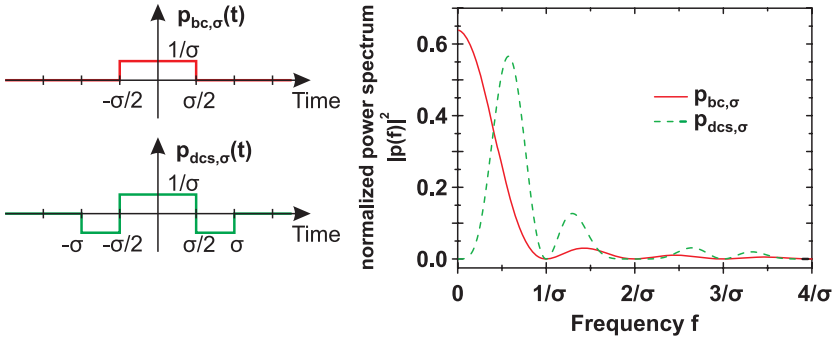


**Figure 5.** Integration pulse shapes $p_{\mathrm{bc},\sigma}(t)$ and $p_{\mathrm{dcs},\sigma}(t)$ and their power spectra $|p_{\mathrm{bc},\sigma}(\omega/2\pi)|^2$ and $|p_{\mathrm{dcs},\sigma}(\omega/2\pi)|^2$. The integrated power spectra have been normalized to unity on the interval $[0, \infty]$.

to the incident photon flux. This flat spectral noise density is filtered and amplified by the detector response $g(\omega)$ (including transit time effects in the photodiodes). Due to its frequency-dependent transimpedance gain $g(\omega)$, the detection electronics allows one to measure signals only within a certain bandwidth. The complex gain characteristics can in principle be extracted directly from the Fourier transform of the pulse response of the detector. When a continuous coherent light beam is applied in a balanced way to the detector, the input noise of light has a flat noise distribution, thus the observed spectral noise density of the electronic output signal can be used directly to determine the modulus of the transimpedance and the detector electronic base noise:

$$|g(\omega)|^2 = \frac{\Omega(\omega) - |e(\omega)|^2}{s_0}. \tag{2}$$

In figure 4(*a*) we show the noise power density $\Omega(\omega/2\pi)$ for Version I of the detector when illuminated with cw balanced light beams at different power levels. We subtract the electronic noise from the data with a known light level incident on the diodes and extract the transimpedance gain $|g(\omega/2\pi)|^2$ of the detector. From figure 4(*b*) we observe that the gain drops by 3 dB at a frequency somewhat below 600 kHz. We also show the ratio of signal noise to electronic noise for input dc light powers of $P = 115$ nW and observe a ratio of 12 dB at low frequencies which drops toward higher frequencies.

To treat the case of pulsed illumination in the frequency domain, the recorded cw-spectrum for white noise input has to be multiplied with the spectrum of the light pulse shape. For a train of independent square pulses $p_{\mathrm{bc},\sigma}(t)$ with duration $\sigma$:

$$p_{\mathrm{bc},\sigma}(t) = \frac{\Theta(t+\sigma/2) - \Theta(t-\sigma/2)}{\sigma}, \tag{3}$$

where

$$\Theta(x) = \begin{cases} 1 & \text{for} \quad x > 0 \\ 0 & \text{for} \quad x \leqslant 0 \end{cases}$$

is the Heaviside step function, the power spectrum is

$$|p_{\mathrm{bc},\sigma}(\omega)|^2 = \left(\frac{\sin(\omega\sigma/2)}{\omega\sigma/2}\right)^2. \tag{4}$$

Assuming now the simple boxcar integration window of duration $\sigma$ given by equation (3) to determine the pulse area, we get the total detected noise power

$$\begin{aligned} P_n &= \int_0^\infty \Omega(\omega)|p(\omega)|^2\,\mathrm{d}\omega \\ &= \int_0^\infty |g(\omega)|^2 s_0 |p(\omega)|^2\,\mathrm{d}\omega + \int_0^\infty |e(\omega)|^2 |p(\omega)|^2\,\mathrm{d}\omega. \end{aligned} \tag{5}$$

Both the temporal shape and the spectrum of the pulse are illustrated in figure 5. Experimentally the noise power is determined from the variance of output pulse areas of a large number of independent pulses. The real expression taking the separation between pulses into account reduces to (5) in the limit of high number of pulses [11]. By using measurements with a spectrum analyzer, we can thus predict the noise scaling expected when using real pulses. The above expression can be used for pulse durations considerably longer than the shaping time. With straightforward modifications also the case of integration windows different from the input pulse length can be treated.

From the spectrum of the boxcar window equation (4), it is clear that especially low-frequency electronic noise such as slow baseline drifts but also the baseline pileup as discussed above will contribute significantly to the total output noise. To circumvent this problem, we change from the boxcar integration window $p_{\mathrm{bc},\sigma}(t)$ to a balanced, double-correlated sampling (dcs) function:

$$p_{\mathrm{dcs},\sigma}(t) = \frac{\Theta(t+\sigma/2) - \Theta(t-\sigma/2)}{\sigma/2} - \frac{\Theta(t+\sigma) - \Theta(t-\sigma)}{\sigma}. \quad (6)$$

The resulting power spectrum

$$|p_{\mathrm{dcs},\sigma}(\omega)|^2 = 4\left(\frac{\sin(\omega\sigma/2)}{\omega\sigma/2} - \frac{\sin(\omega\sigma)}{\omega\sigma}\right)^2 \quad (7)$$

has no contribution at $\omega = 0$. The pulse shape $p_{\mathrm{dcs},\sigma}(t)$ and its power spectra are also illustrated in figure 5. Using an integration function as $p_{\mathrm{dcs},\sigma}(t)$ thus reduces the influence of low-frequency noise contributions and allows one to cancel the effect of baseline pulling. Generally, the integration with a certain gating function $p(t)$ can be understood as frequency (band) pass filtering of the signal with the power spectrum of the gating function $|p(\omega)|^2$. In the particular case of $p_{\mathrm{dcs}}$, the window function is similar to that used for the double-correlated sampling which is routinely applied in CCD camera readout units in order to reduce correlated noise sources.

### 3.2. Noise in pulsed operation

In a typical experimental application, we use $k$ light pulses $p_i$ of duration $\tau$ of the order of some microseconds and repetition period $r$ of the order of some tens of microseconds [7] (compare figure 1). The electronic differential detector signal $S(t)$ is acquired on a storage oscilloscope and integrated with the gating function $p_{\mathrm{bc},\sigma}(t)$ or $p_{\mathrm{dcs},\sigma}(t)$ to give the pulse area normalized to its duration. Time delays, e.g. from the response time, from the pulsing device are taken into account by a time translation $t \to t - t_0$ of the integration window. In general, both the duration of the integration window $\sigma$ and its position in time have to be optimized for each detector/experimental set-up. After the integration, we are left with the pulses $p_i$:

$$p_i = \int_{-\infty}^{+\infty} p_{\mathrm{bc},\sigma}(t)S(t)\,\mathrm{d}t = \frac{1}{\sigma}\int_{t_0+(i-1)r}^{t_0+(i-1)r+\sigma} S(t)\,\mathrm{d}t \quad (8)$$

of which we calculate the variance $\delta^2 p \equiv \frac{1}{k}\sum_{i=1}^{k}\left(p_i^2 - \left(\frac{1}{k}\sum_{i=1}^{k} p_i\right)^2\right)$ to evaluate the noise of the signal.

*3.2.1. Baseline subtraction* When an imbalanced signal is being measured, the baseline pulling encountered in figure 2 has to be taken into account. When we use the double-correlated sampling gating function $p_{\mathrm{dcs},\sigma}(t)$ we obtain

$$\begin{aligned} p_i' &= \int_{-\infty}^{+\infty} p_{\mathrm{dcs}}(t)S(t)\,\mathrm{d}t \\ &= \frac{1}{\sigma}\left(\int_{t_0+(i-1)r}^{t_0+(i-1)r+\sigma} S(t)\,\mathrm{d}t\right) \\ &\quad - \frac{1}{\sigma}\left(\int_{t_0+(i-1)r-\sigma/2}^{t_0+(i-1)r} S(t)\,\mathrm{d}t + \int_{t_0+(i-1)r+\sigma}^{t_0+(i-1)r+3\sigma/2} S(t)\,\mathrm{d}t\right) \\ &\equiv p_i - b_i. \end{aligned} \quad (9)$$

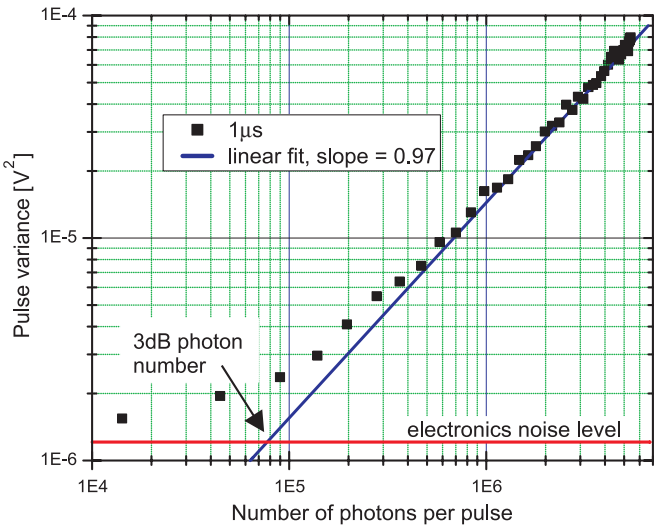


**Figure 6.** Pulse variance for different pulse photon numbers. The data have been analyzed using the simple boxcar gating function $p_{\mathrm{bc},\sigma}$ with a $\sigma = 1.25$ $\mu$s integration window around a $\tau = 1$ $\mu$s initial light pulse. The slope of the linear fit in the log–log plot to the light noise dominated part is 1, confirming that the observed noise is light shot noise. The 3 dB photon number $n_{3\mathrm{dB}} = 8 \times 10^4$ corresponds to an rms electronic noise of ENC = 280 electrons in the integration window.

It is clear that integrating $S(t)$ with $p_{\mathrm{dcs},\sigma}(t)$, i.e., also before and after acts as to subtract the mean of two signal baseline intervals before and after the light pulse. Since, in order to extract an estimate for the baseline level, the output signal of the detector is in total integrated over a longer time $2\sigma$ than for the simple boxcar window function, the contribution of high-frequency electronic noise to the total noise *energy* of a pulse area signal is increased. Depending on the detailed behavior of the low-frequency noise spectrum and under the constraints given by the desired pulse repetition rate in an experiment, the shape and duration of the baseline sampling interval can be optimized to minimize the additional contribution of the electronic noise. The double-correlated sampling discussed can be understood as taking the two sample variances on the dark detector electronic signal, thus removing correlations in the bare detector signal [12].

## 4. Detector performance

Within the framework presented above, we now analyze the performance of the different detector versions. As a figure of merit, we consider the electronic noise equivalent light shot noise, i.e., the number of photons per light pulse required to generate the same noise as the detection electronics has intrinsically (3 dB level). This photon number can then be converted into the equivalent noise charge (ENC) which is just the corresponding standard deviation. To determine this level, we send balanced pulse trains of several hundred light pulses onto the detector, evaluate the variance of the integrated signal and plot the variance as a function of the mean photon number in each pulse. The result for $\tau = 1$ $\mu$s pulse duration is shown in figure 6. Here we have used the simple integration gating function $p_{\mathrm{bc},\sigma}(t)$. The scaling of the pulse variance data with

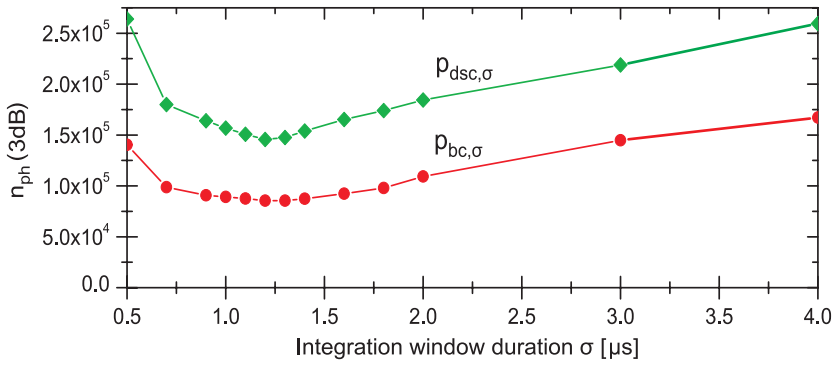


**Figure 7.** By varying the duration of the integration window and its position with respect to the pulse, the optimal integration parameters can be determined. When using the simple boxcar window function, we find the optimal integration duration at $\sigma = 1.25\ \mu$s with a 3 dB photon number of $n_{3\mathrm{dB}} \sim 0.8 \times 10^5$. When implementing baseline subtraction via the gating function $p_{\mathrm{dcs},\sigma}(t)$, the 3 dB noise level rises by a factor of 2, $n_{3\mathrm{dB}} \sim 1.6 \times 10^5$. The additional electronic noise contribution when using $p_{\mathrm{dcs},\sigma}(t)$ is due to the increased total signal integration time.

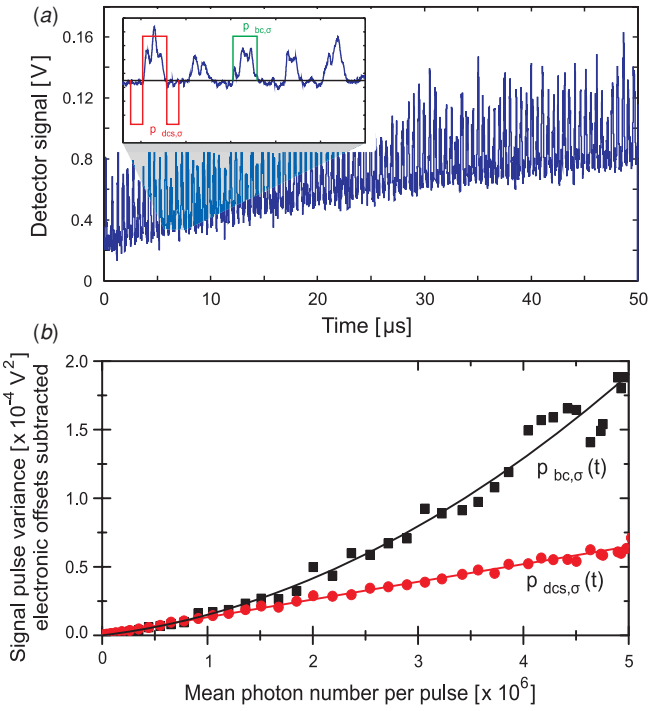


**Figure 8.** (*a*) Due to technical imperfections in the pole/zero cancellation of the Gaussian filter, the detector baseline piles up when the incident light pulses are not fully balanced. (*b*) When analyzing the signal from an imbalanced input, the variance of pulses integrated with the simple integration gating function $p_{\mathrm{bc}}$ shows a clear contribution of classical-correlated noise. Using the baseline subtracting window function $p_{\mathrm{dcs}}$, the linear scaling characteristic for shot noise is regained. In both data sets, the electronic noise level has been subtracted.

mean photon number per pulse in a log–log plot shows a slope of 1 which confirms that the observed noise is due to light shot noise. The optimal integration window $p_{\mathrm{bc},\sigma}(t)$ is found by optimizing the 3 dB photon number with respect to the window duration $\sigma$.

In figure 7, the optimization procedure is illustrated for both integration gating functions $p_{\mathrm{bc},\sigma}(t)$ and $p_{\mathrm{dcs},\sigma}(t)$. Evidently, the optimum duration of the integration window for short pulses is governed by the shaping time. When the pulse integration window is very short, the electronic noise is very large compared to the light noise in the time window, thus the 3 dB level is rather high. When the integration window is much longer than the actual light pulse, the ratio of light shot noise to electronic noise is artificially decreased and therefore the 3 dB level rises again. The optimal value is found at approximately the initial pulse duration plus twice the shaping time. The optimal noise data for Version I of the detector are $n_{3\mathrm{dB}} = 8 \times 10^4$ electronic noise equivalent photon number for pulses shorter than the shaping time, i.e., durations $<1.5\ \mu$s. Version II performs almost equally well with $n_{3\mathrm{dB}} = 1.2 \times 10^5$ photons per microsecond. With quantum efficiency of the employed photodiodes exceeding 90%, the photon numbers can be converted to the more familiar equivalent noise charge yielding ENC = 280 electrons for Version I and ENC = 340 electrons for Version II when applying light pulses of up to $\tau \lessapprox 1\ \mu$s duration. Both values are very close to those expected for the employed front-end amplifier components. We attribute this improvement compared to [6] to a very careful choice of the electric components and a careful circuit layout together with the analysis presented here. Specifically, photon numbers of $n \gtrsim 10^5$ can reliably be detected at the shot noise level. The 3 dB levels have been confirmed by an analysis of cw noise power density spectra whereof examples have been shown in figure 4. By analyzing these according to formula (5), the expected noise performance in pulsed operation can be inferred and agreement between the values obtained from both approaches confirms that, e.g., transient effects due to light pulse switching do not affect the detector performance.

As discussed above, the balancing of the detector may change during the measurement and the resulting electronic signal pileup may make a baseline subtraction by using the double-correlated sampling window function $p_{\mathrm{dcs},\sigma}$ necessary. Figure 8(*a*) shows the effect of baseline pileup for a train of slightly imbalanced input signals. The noise scaling results for the two gating functions $p_{\mathrm{bc},\sigma}(t)$ and $p_{\mathrm{dcs},\sigma}(t)$ are compared in figure 8(*b*). When applying the simple integration function $p_{\mathrm{bc},\sigma}(t)$, a clear quadratic (classical) noise contribution can be observed. In contrast, when the double-correlated sampling $p_{\mathrm{dcs},\sigma}(t)$ is employed, the linear scaling and thus shot noise limited performance is observed. The linear part of the data

obtained with $p_{\mathrm{bc},\sigma}(t)$, i.e. its light shot noise contribution, corresponds exactly to the light shot noise level extracted with $p_{\mathrm{dcs},\sigma}(t)$.

The price paid for using double-correlated sampling is that one unit of electronic noise is added. By comparing the 3 dB photon number level in figure 6, $n_{3\mathrm{dB}} = 0.8 \times 10^5$ obtained with $p_{\mathrm{bc},\sigma}(t)$ for a balanced signal with the level $n_{3\mathrm{dB}} = 1.6 \times 10^5$ extracted in figure 7 with the double-correlated sampling window, we observe this additional electronic noise contribution from the analysis. In our typical experiments, we use photon numbers per pulse $n \approx 10^7$ which renders the electronic noise negligible [7]. We also implement the double-correlated sampling integration function in order to compensate for detector imperfections. The best performance of the detector is, of course, reached when baseline subtraction is not necessary, i.e., when the detector is balanced all the time. For very high photon numbers, e.g. $n > 10^8$ per pulse, the shot noise alone can create an imbalance which in turn may pull the baseline significantly. Therefore, in this case, baseline subtraction is compulsory. On the other hand, in this regime the electronic noise is much lower than the shot noise of light, and consequently, additional unit of electronic noise is of little importance.

## 5. Conclusion

We have presented the working principle of ultra low-noise differential integrating AC photodetectors and discussed two different hardware realizations with components from different suppliers. The cw and pulsed noise performance of both detectors has been discussed in detail with special emphasis on the analysis procedures for pulsed operations. We have demonstrated that the ultra low-noise performance of our detectors extends into the range of microsecond long pulses which is of considerable importance for atomic physics applications [7]. There, duration and photon number per pulse are set by the desired coupling strength between the light pulses and the atomic ensemble and are typically in the range of $10^5$–$10^6$ photons distributed over a few microseconds. In this regime the noise performance of the detectors discussed here is considerably better than what has been previously reported [6]. The influence of correlated noise sources has been discussed, for example classical pulse correlations generated by the pulling of the detector baseline for imbalanced detector operation. A baseline subtraction scheme has been proposed and successfully used to circumvent these shortcomings. Correction for the baseline pulling is generally only necessary when rather high photon numbers are considered. In this case, the additional electronic noise due to the analysis procedure is negligible compared to the detected light shot noise.

## Acknowledgments

This work was funded by the Danish National Research Foundation as well as the EU grants QAP and EMALI.

## References

[1] Chaudhury S, Smith G A, Schulz K and Jessen P S 2006 Continuous nondemolition measurement of the Cs clock transition pseudospin *Phys. Rev. Lett.* **96** 043001
[2] Usami K and Kozuma M 2007 Observation of a topological and parity-dependent phase of $m = 0$ spin states *Phys. Rev. Lett.* **99** 140404
[3] de Echaniz S R, Mitchell M W, Kubasik M, Koschorreck M, Crepaz H, Eschner J and Polzik E S 2005 Conditions for spin squeezing in a cold $^{87}$ Rb ensemble *J. Opt. B: Quantum Semiclass. Opt.* **7** S548
[4] Windpassinger P J, Oblak D, Petrov P G, Kubasik M, Saffman M, Garrido Alzar C L, Appel J, Müller J-H, Kjærgaard N and Polzik E S 2008 Nondestructive probing of Rabi oscillations on the cesium clock transition near the standard quantum limit *Phys. Rev. Lett.* **100** 103601
[5] Hilliard A, Kaminski F, Le Targat R, Olausson C, Polzik E S and Müller J-H 2008 Rayleigh superradiance and dynamic Bragg gratings in an end-pumped Bose–Einstein condensate *Phys. Rev.* A **78** 051403
[6] Hansen H, Aichele T, Hettich C, Lodahl P, Lvovsky A, Mlynek J and Schiller S 2001 Ultrasensitive pulsed, balanced homodyne detector: application to time-domain quantum measurements *Opt. Lett.* **26** 1714
[7] Appel J, Windpassinger P J, Oblak D, Busk Hoff U, Kjaergaard N and Polzik E S 2008 Mesoscopic atomic entanglement for precision measurements beyond the standard quantum limit arXiv:0810.3545
[8] Bertuccio G and Pullio A 1993 A method for the determination of the noise parameters in preamplifying systems for semiconductor radiation detectors *Rev. Sci. Instrum.* **64** 3294
[9] Scully M O and Zubairy M S 1997 *Quantum Optics* (Cambridge: Cambridge University Press)
[10] Reif F S 1965 *Fundamentals of Statistical and Thermal Physics* (New York: McGraw-Hill)
[11] Barnes J *et al* 1971 Characterization of frequency stability *IEEE Trans. Instrum. Meas.* **IM-20** 105
[12] Allan D W 1966 Statistics of atomic frequency standards *Proc. IEEE* **54** 221